m^{6}A-modified HOXC10 promotes HNSCC progression via co-activation of ADAM17/EGFR and Wnt/β-catenin signaling

YUJUAN ZHOU[1*], QIANG HUANG[1*], CHUNPING WU[1*], YE XU[2], YANG GUO[1], XIAOHUI YUAN[1], CHENGZHI XU[1] and LIANG ZHOU[1]

[1]Department of Otorhinolaryngology, Eye and ENT Hospital, Fudan University, Shanghai 200031; [2]Liver Cancer Institute, Zhongshan Hospital, Fudan University and Key Laboratory of Carcinogenesis and Cancer Invasion, Ministry of Education, Shanghai 200032, P.R. China

Received July 25, 2023; Accepted October 12, 2023

DOI: 10.3892/ijo.2023.5598

Abstract. The homeobox (HOX) gene family plays a fundamental role in carcinogenesis. However, the oncogenic mechanism of HOXC10 in head and neck squamous cell carcinoma (HNSCC) remains unclear. In the present study, it was revealed that HOXC10 expression was significantly higher in HNSCC tissues than in adjacent tissues, and a high level of HOXC10 was closely associated with worse clinical outcomes. HOXC10 overexpression promoted HNSCC cell proliferation, migration, and invasion, both *in vitro* and *in vivo*. Mechanistically, chromatin immunoprecipitation sequencing revealed that HOXC10 drove the transcriptional activation of a disintegrin and metalloproteinase 17 (ADAM17), and the ADAM17/epidermal growth factor receptor (EGFR)/ERK1/2 signaling pathway facilitating the proliferation of HNSCC. Furthermore, mass spectrometric analysis indicated that HOXC10 interacted with ribosomal protein S15A (RPS15A) and enhanced RPS15A protein expression, activating the Wnt/β-catenin pathway and contributing to invasion and metastasis of HNSCC. Additionally, the methylated RNA immune precipitation and RNA antisense purification assays showed that *N*^{6}-methyladenosine (m^{6}A) writer, methyltransferase-like 3, catalyzed m^{6}A modification of the HOXC10 transcript, m^{6}A reader insulin like growth factor 2 mRNA binding protein (IGF2BP)1 and IGF2BP3 involved in recognizing and stabilizing m^{6}A-tagged HOXC10 mRNA. In summary, the present study identified HOXC10 as a promising candidate oncogene in HNSCC. The m^{6}A modification-mediated HOXC10 promoted proliferation, migration, and invasion of HNSCC through co-activation of ADAM17/EGFR and Wnt/β-catenin signaling, providing a novel diagnostic and prognostic biomarker and a potential therapeutic target for HNSCC.

Correspondence to: Professor Liang Zhou or Dr Chengzhi Xu, Department of Otorhinolaryngology, Eye and ENT Hospital, Fudan University, 83 Fenyang Road, Xuhui, Shanghai 200031, P.R. China
E-mail: liang.zhou@fdeent.org
E-mail: chengzhi_xu@fudan.edu.cn

*Contributed equally

Key words: homeobox C10, head and neck squamous cell carcinoma, a disintegrin and metalloproteinase 17, ribosomal protein S15A, N6-methyladenosine

Introduction

Head and neck squamous cell carcinoma (HNSCC) is one of the most common malignancies in the world. Globally, >700,000 cases of HNSCC are newly diagnosed, and >300,000 patients with HNSCC succumb to this disease each year (1). Despite multimodality treatments, recurrence and metastasis of HNSCC develop in numerous patients. Therefore, revealing the underlying molecular mechanism of HNSCC progression and identifying new key targets for the diagnosis and treatment of HNSCC are especially urgent.

Homeobox C10 (HOXC10) is a member of the HOX genes, which include four clusters: HOXA, HOXB, HOXC, and HOXD (2). Accumulated evidence has indicated that the HOX gene family is markedly expressed in various cancers and plays an important role in cancer progression. For example, pharmacologic inhibition of HOXA9 suppressed TWIST1-induced aggressive cellular phenotypes of prostate cancer *in vitro* and metastasis *in vivo* (3). Higher HOXB8 expression in ovarian serous carcinoma effusions was associated with significantly shorter overall survival in post-chemotherapy patients (4). Invasive and metastatic potential of cancer cells were enhanced by HOXD3 through the TGF-β-dependent and -independent pathways (5). The HOXC10 gene is located on chromosome 12 and plays an important role in embryonic morphogenesis and cellular identity (6). Pathiraja *et al* showed that aromatase inhibitor treatment of breast cancer resulted in downregulation of HOXC10 expression via methylation of HOXC10 promoter regions and confers inhibitors resistance (7). Moreover, another study reported that HOXC10 overexpression promoted angiogenesis in glioma via upregulation of VEGFA expression and interaction with PRMT5 (8). HOXC10 may become a useful marker in the diagnosis or treatment evaluation of cancer. However, to date, only a limited number of studies have focused on the role of HOXC10 in the pathogenesis of HNSCC. The biologic mechanisms of HOXC10 in HNSCC remain unclear, and further study is required.

In the present study, the expression and biological functions of HOXC10 were determined using HNSCC samples and animal models. In particular, the underlying mechanisms of HOXC10-induced proliferation, invasion, and metastasis of HNSCC were also elucidated. Furthermore, it was found that the N^6-methyladenosine (m^6A) writer, methyltransferase-like 3 (METTL3), and the m^6A readers, insulin like growth factor 2 mRNA binding protein (IGF2BP)1 and IGF2BP3 participated in increasing the stability of the HOXC10 transcript in HNSCC.

Materials and methods

Antibodies and reagents. Antibodies used for western blot analysis were as follows: Anti-HOXC10 (1:1,000; cat. no. A303-178A-M; Thermo Fisher Scientific, Inc.), anti-β-actin (1:1,000; cat. no. ab8224; Abcam), anti-E-cadherin (1:1,000; cat. no. 3195), anti-N-cadherin (1:1,000; cat. no. 13116), anti-vimentin (1:1,000; cat. no. 5741) and anti-Snail (1:1,000; cat. no. 3879; all from Cell Signaling Technology, Inc.), anti-ADAM17 (1:1,000; cat. no. ab39162), phosphorylated (p)-ERK1/2 (1:1,000; cat. no. ab278538), anti-ERK1/2 (1:1,000; cat. no. ab184699), anti-p-epidermal growth factor receptor (EGFR) (1:1,000; cat. no. ab40815) and anti-EGFR (1:1,000; cat. no. ab52894; all from Abcam), anti-RPS15A (1:1,000; cat. no. A304-990A; Thermo Fisher Scientific, Inc.), anti-Axin2 (1:1,000; cat. no. ab109307), anti-MMP7 (1:1,000; cat. no. ab207299), anti-c-Myc (1:1,000; cat. no. ab32072), anti-β-catenin (1:1,000; cat. no. ab32572), anti-histone H3 (1:1,000; cat. no. ab1791), anti-METTL3 (1:1,000; cat. no. ab195352), anti-IGF2BP1 (1:1,000; cat. no. ab184305) and anti-IMP3 (1:1,000; cat. no. ab177477; all from Abcam). The following antibodies were used for immunohistochemistry: Anti-HOXC10 (1:500; cat. no. ab153904; Abcam), anti-E-cadherin (1:400; cat. no. 3195; Cell Signaling Technology, Inc.), anti-vimentin (1:400; cat. no. 5741; Cell Signaling Technology, Inc.), and anti-Snail (1:1,000; cat. no. ab85936; Abcam). Anti-HOXC10 (1:100; cat. no. A303-178A) and anti-RPS15A (1:100; cat. no. A304-990A; both from Thermo Fisher Scientific, Inc.) were used for immunoprecipitation (IP). Actinomycin D was obtained from MedChemExpress.

Patients and specimens. HNSCC tissues and para-carcinoma tissues were obtained from 77 patients diagnosed with HNSCC from the Eye and ENT Hospital, Fudan University (Shanghai, China), from November 2017 to March 2022. There were 75 males and 2 female patients, aged 43-84 years, with a mean age (± standard deviation) of 64.4±9.3 years. The inclusion criteria were as follows: Patients who were diagnosed with primary HNSCC, had available tumor tissue samples suitable for tissue microarray (TMA) construction, and had complete clinical and pathological data. Patients who had received prior chemotherapy, immunosuppressive therapy, or had severe comorbidities or medical conditions were excluded from the study. The tissues were stored at -80˚C until their use. Neoplastic and matched normal tissues were used for TMA construction. Pannoramic MIDI (3DHISTECH, Ltd.) was then used to scan the microarray. The present study was authorized by the Ethics Committee of the Eye and ENT Hospital of Fudan University (approval. no. 2018036). These patients had received no treatment before surgery. All patients provided written informed consent.

Cell culture. The human HNSCC cell lines, Tu686 and FaDu (The Cell Bank of Type Culture Collection of The Chinese Academy of Sciences), were used in the present study. HuLa-PC (CRL-3342; ATCC), a human normal laryngeal cell line, was also used in the present study. Tu686 was cultured using RPMI-1640 medium (HyClone; Cytiva) supplemented with 10% fetal bovine serum (FBS; Gibco; Thermo Fisher Scientific, Inc.) and 1% penicillin-streptomycin. FaDu and HuLa-PC was cultured in Dulbecco's modified Eagle's medium (DMEM; HyClone; Cytiva) supplemented with 10% FBS and 1% penicillin-streptomycin. All cells were placed in an incubator with 5% CO_2 at 37˚C. AMC-HN8 cells were a kind gift from Professor Sang Yoon Kim of Samsung Medical Center (Seoul, Korea). Tu212 and M4E cell lines were obtained from Central South University (Changsa, China). AMC-HN8, Tu212 and M4E were cultured using RPMI-1640 medium (HyClone; Cytiva) supplemented with 10% and 1% penicillin-streptomycin, and were placed in an incubator with 5% CO_2 at 37˚C. For the mRNA stability assay, transfected HNSCC cells were treated with Actinomycin D (5 μg/ml; cat. no. S8964; Selleck Chemicals) at 37˚C for 0, 3 and 6 h prior to RNA isolation.

Reverse transcription-quantitative PCR (RT-qPCR). Total RNA was extracted from cell lines and tissues using Trizol® reagent (Invitrogen; Thermo Fisher Scientific, Inc.), and then was reverse-transcribed into cDNA using a RevertAid First Strand cDNA Synthesis kit (cat. no. K1622; Thermo Fisher Scientific, Inc.) according to the manufacturer's instructions. The resulting cDNA was amplified with a gene-specific primer and a qPCR SYBR Green Master Mix kit (Shanghai Yeasen Biotechnology Co., Ltd.). The PCR reaction involved an initial denaturation step at 95˚C for 5 min followed by 40 cycles of denaturation at 95˚C for 10 sec, annealing at 55-60˚C for 20 sec, and extension at 72˚C for 20 sec. The primer sequences are listed in Table I. The relative expression levels of the target genes were normalized to β-actin and reported as $2^{-\Delta\Delta Cq}$ (9). In addition, HNSCC cells were treated with 5-AZA-CdR (cat. no. S1200; Selleck Chemicals) at 1 μM for 48 h, and the HOXC10 mRNA level was examined using RT-qPCR.

Western blot analysis. Total proteins were extracted using RIPA lysis buffer containing 1% phenylmethanesulfonyl fluoride (PMSF; Beyotime Institute of Biotechnology). The protein concentration was detected using a BCA protein assay (Beyotime Institute of Biotechnology). A total of ~20 μg protein/lane was separated by 6-12% SDS-PAGE and then transferred onto a PVDF membrane (MilliporeSigma). Subsequently, the membranes were blocked using 5% nonfat milk for 1 h at room temperature, and then incubated with the primary antibodies at 4˚C overnight. The following day, secondary antibodies: HRP-labeled goat anti-rabbit IgG (H+L) (cat. no. A0208; 1:1,000) and HRP-labeled goat anti-mouse IgG (H+L) (cat. no. A0216; 1:1,000), provided by Beyotime Institute of Biotechnology, were used to incubate the membranes at room temperature for 1 h. Target protein bands were finally visualized using an ECL system (MilliporeSigma). β-actin served as the control.

Table I. Sequences of primers.

Gene symbol	Forward primer (5'-3')	Reverse primer (5'-3')
HOXC10	AGCCTCGCCCTCAACACCTATC	GCAGCAGACATTCTCCTCCTTGAC
MMP7	GAGGATGAACGCTGGACGGATG	AGGATCAGAGGAATGTCCCATACCC
Myc	AGCAGCGACTCTGAGGAGGAAC	TCCAGCAGAAGGTGATCCAGACTC
Axin2	CACCACCACCATTCGCAGTACC	ACATGCTTCGTCGTCTGCTTGG
METTL3	TGCCTTTGCCAGTTCGTTAGTCTC	ACTGACCTTCTTGCTCTGTTGTTCC
IGF2BP1	CACCCGAAACACCTGACTCCAAAG	GCCATAGATTCTTCCCTGAGCCTTG
IGF2BP3	TCACTTCTATGCTTGCCAGGTTGC	CCTTCTGTTGTTGGTGCTGCTTTAC
RPS15A	AACCTCACAGGCAGGCTAAACAAG	TGGCGGGATGGAAGCAGATTATTC
ADAM17	AGCAGATTCGCATTCTCAAGTCTCC	GCAACATCTTCACATCCCAAGCATC
β-actin	GCACTCTTCCAGCCTTCCTTCC	GCGGATGTCCACGTCACACTTC

HOXC10, homeobox C10; METTL3, methyltransferase-like 3; IGF2BP1, insulin like growth factor 2 mRNA binding protein 1; IGF2BP3, insulin like growth factor 2 mRNA binding protein 3; RPS15A, ribosomal protein S15A; ADAM17, a disintegrin and metalloproteinase 17.

Cell migration, invasion, and proliferation assays. Cellular migration and invasion abilities were determined in 24-well Transwell chambers (Corning, Inc.). For migration assays, $5x10^4$ cells with 200 μl of serum-free media were added to the upper chamber, whereas 600 μl of complete media (RPMI-1640 medium supplemented with 10% FBS) was added to the bottom chamber. After 24 h at 37˚C, the cells in the lower chambers were fixed and stained with crystal violet (Beyotime Institute of Biotechnology) for 30 min at room temperature. For the invasion assays, a polycarbonate membrane was pre-coated with Matrigel (Corning, Inc.) at 37˚C for 3 h. For quantification, a light microscope (Leica Microsystems GmbH) was used to analyze the number of cells.

5-Ethynyl-2'-deoxyuridine (EdU) assay was performed to evaluate the ability of cellular proliferation based on the BeyoClick™ EdU Cell Proliferation Kit with Alexa Fluor 555 (cat. no. C0075S; Beyotime Institute of Biotechnology). The transfected cells were seeded into 24-well plates ($5x10^3$ cells/well). The cells were cultured in EdU (10 μM) for 2 h at 37˚C and then fixed with 4% paraformaldehyde for 10 min at room temperature. Subsequently, the samples were stained with the kit at room temperature for 1 h, according to the manufacturer's instructions. Images were detected using a fluorescence microscope (Leica Microsystems GmbH).

Co-immunoprecipitation (Co-IP) and ubiquitination assays. Proteins were extracted using 450 μl IP lysis buffer (Thermo Fisher Scientific, Inc.) containing 1% PMSF (Beyotime Institute of Biotechnology). Following cell lysis the supernatant was collected by centrifugation at 12,000-16,000 x g for 10 min at 4˚C) and then incubated with the primary antibodies on a shaker at 4˚C overnight. Subsequently, the samples were incubated overnight with protein A/G magnetic beads (cat. no. LSKMAGAG02; MilliporeSigma). The beads were then washed 3 times with lysis buffer (cat. no. 87788; Thermo Fisher Scientific, Inc.) and then boiled at 100˚C in loading buffer for 30 min for subsequent western blot analysis assays.

For ubiquitination (Ubi) assays, transfected HNSCC cells were treated with MG132 (5 μmol; Selleck Chemicals) at 37˚C for 4 h before being harvested. The cell lysates were immunoprecipitated with the RPS15A antibody (cat. no. A304-990A; Thermo Fisher Scientific, Inc.) and analyzed by western blotting with ubiquitin antibody (cat. no. sc8017; Santa Cruz Biotechnology, Inc.) at 4˚C overnight.

Transfection. For transient cell transfection, siRNAs against human ADAM17 (5'-ACUUCACACUGUACUCGCUTT-3'), RPS15A (5'-GAUGAUGAAGCAUGGUUACAU-3'), METTL3 (5'-CUGCAAGUAUGUUCACUAUGA-3'), IGF2BP1 (5'-GGCTCAGTATGGTACAGTA-3'), IGF2BP3 (5'-GCTGAGAAGTCGATTACTA-3') and the control siRNAs (5'-TTCTCCGAACGTGTCACGT-3') were obtained from Genomeditech (Shanghai) Co., Ltd. The RPS15A overexpression plasmid (Fig. S1A), ADAM17 overexpression plasmid (Fig. S1B), and empty plasmids were purchased from Genomeditech (Shanghai) Co., Ltd. The siRNAs (50 nM) or plasmids (2 μg/ml) were transfected using Lipofectamine® 2000 (Thermo Fisher Scientific, Inc.) at 37˚C (for siRNAs, 48 h and plasmids, 6 h). For stable cell transfection (at 37˚C for 18-20 h), the HOXC10 overexpression and knockdown lentivirus (5'-ACCTAGTGTCAAGGAGGAGAA-3') were obtained from Genomeditech (Shanghai) Co., Ltd. The 3rd generation system was used and the interim cell line used was 293T (ATCC). The quantity of lentiviral plasmid that was used was 20 μg, for transfection, and the ratio used for the lentivirus, packaging and envelope plasmids was: 3:1:1. The medium was collected by centrifugation at 500 x g for 5 min at 4˚C at a multiplicity of infection of 10. The duration of transfection into the cells of interest was 16 h and the time interval between transduction and subsequent experimentation was ~2 weeks. To create stable cell lines, the selection method used was puromycin (5 μg/ml), and the concentration of puromycin used for maintenance was 2 μg/ml.

Immunofluorescence. The cells were fixed with 4% paraformaldehyde (Beyotime Institute of Biotechnology) at room temperature for 15 min. and then permeabilized with 0.2% Triton X-100 (Beyotime Institute of Biotechnology). Subsequently, the cells were blocked using 1% BSA at room

temperature for 1 h and then incubated with the primary antibodies at 4˚C overnight. The following day, the cells were incubated with fluorescent secondary antibodies at room temperature for 1 h. The stained cells were analyzed using a Leica microscope (Leica Microsystems GmbH). The following primary antibodies were used for immunofluorescence: Anti-HOXC10 (1:100; cat. no. ab153904; Abcam), anti-E-cadherin (1:1,000; cat. no. 3195; Cell Signaling Technology, Inc.), anti-vimentin (1:100; cat. no. 5741; Cell Signaling Technology, Inc.), anti-Snail (1:100; cat. no. A5243; ABclonal), anti-RPS15A (1:100; cat. no. DF9117; Affinity Biosciences), and anti-β-catenin (1:200; cat. no. ab32572; Abcam). The fluorescent secondary antibodies used were as follows: Alexa fluor 488-labeled goat anti-mouse IgG (H+L) (1:500; cat. no. A0428) and Alexa fluor 555-labeled donkey anti-rabbit IgG (H+L) (1:500; cat. no. A0453; both from Beyotime Institute of Biotechnology).

Immunohistochemistry. Tissues were fixed with 4% paraformaldehyde at room temperature for 24 h. and then embedded in paraffin. The paraffin-embedded tissues were sectioned into 4-μm thick slices. Tissue slices were deparaffinized, rehydrated, blocked with 10% goat serum (cat. no. C0265; Beyotime Institute of Biotechnology) at 37˚C for 60 min, and then incubated overnight with primary antibodies at 4˚C. Subsequently, the slices were incubated with secondary antibodies [HRP-labeled goat anti-mouse IgG (H+L) (1:50; cat. no. A0216) and HRP-labeled goat anti-rabbit IgG (H+L) (1:50; cat. no. A0208; both from Beyotime Institute of Biotechnology] and stained with DAB. The slides were analyzed using a light microscope (Leica Microsystems GmbH). The histochemistry score (H-Score) value was calculated using Image-Pro Plus software 6.0 and used as an indicator of the level of protein.

Dual-luciferase reporter assay. The lentivirus-transfected cells were seeded in 24-well plates. ADAM17 promoter plasmids [Genomeditech (Shanghai) Co., Ltd.] were transfected into these cells. After 48 h of transfection using Lipofectamine 2000 (cat. no. 11668019; Thermo Fisher Scientific, Inc., the relative luciferase activity of reporter vectors was analyzed using a Dual-Luciferase Reporter Gene Assay kit (cat. no. RG027; Beyotime Institute of Biotechnology) following the manufacturer's protocols. The luciferase activity against that of *Renilla* was measured.

RNA antisense purification (RAP) assay. In this experiment, a RAP assay was performed using a RAP kit (cat. no. Bes5103-1-S; Guangzhou Bersinbio Co., Ltd.), following the manufacturer's protocols and as previously described (10,11). The biotin-labeled specific probe was used to pull down the target RNA. RNAs and proteins that interacted with the target RNA were also obtained. The RNA products were then analyzed by RT-qPCR, and the protein products were analyzed by western blotting.

Methylated RNA immune precipitation (MeRIP). Total RNA was extracted using TRIzol reagent (Invitrogen; Thermo Fisher Scientific, Inc.). The RNAs were cleaved into RNA fragments. The fragmented RNAs were immunoprecipitated with an anti-m^{6}A antibody (included in a MeRIP kit; cat. no. Bes5203-2; Bersinbio). Protein A/G magnetic beads (20 μl per IP; included in the aforementioned kit) were added to the mixture at 4˚C, overnight. The beads were washed three times with an elution buffer. The RNAs were extracted using phenol-chloroform-isoamylol (included in the aforementioned kit; 25:24:1). The expression of the RNA was then analyzed by RT-qPCR.

Animal experiments. A total of 20 male BALB/c nude mice (4-6 weeks old; weight, 18-20 g) were obtained from the Shanghai SLAC Laboratory Animal Co., Ltd. The present study was performed according to the guidelines of the National Institutes of Health for the Care and Use of Laboratory Animals (12). Mice were housed in animal rooms with a 10-h light/14-h dark cycle and at a constant temperature (22-27˚C). Animals had free access to standard rodent chow and water. For the subcutaneous xenograft tumor model, transfected cells ($5x10^6$) were injected on the sides of the flanks of mice (n=5 per group). Subsequently, 30 days later, the mice were euthanized by cervical dislocation following anesthesia induced by intraperitoneal injection of 0.3% sodium pentobarbital (30 mg/kg). Euthanasia was confirmed by verifying respiratory and cardiac arrest, along with pupil dilation, for a minimum of 10 min. Tumor size and tumor weight were measured (max tumor diameter, 9.6 mm; max area, 82.56 mm^2; max volume, 355.01 mm^3). For the pulmonary metastasis model, transfected cells ($2x10^6$) were injected into the mouse tail veins (n=5 per group). Subsequently, 60 days later, the mice were sacrificed, and lungs were obtained. Finally, lung and tumor tissues were available for H&E staining at room temperature for 5 min or immunohistochemistry staining. All animal procedures were approved (approval no. 202212201) by the Eye and ENT Hospital, Fudan University (Shanghai, China).

RNA sequencing. Total RNA was extracted using the TRIzol reagent (cat. no. 15596018CN; Invitrogen; Thermo Fisher Scientific, Inc.) according to the manufacturer's protocol. RNA purity and quantification were evaluated using a NanoDrop 2000 spectrophotometer (Thermo Fisher Scientific, Inc.). RNA integrity was assessed using the Agilent 2100 Bioanalyzer (Agilent Technologies, Inc.). The libraries were then constructed using NEBNext®Ultra™ RNA Library Prep Kit for Illumina® (New England BioLabs, Inc.) following manufacturer's recommendations. The transcriptome sequencing and analysis were conducted by Orizymes Biotechnologies (Shanghai) Co., Ltd. The libraries were sequenced on an Illumina HiSeq X Ten platform and 150-bp paired-end reads were generated. Raw data (raw reads) of fastq format (https://maq.sourceforge.net/fastq.shtml.) were firstly processed using Trimmomatic (http://www.usadellab.org/cms/index.php?page=trimmomatic). Clean data were obtained for downstream analyses by removing reads containing adapter, reads containing ploy-N and low-quality reads from raw data. The clean reads were mapped to the human genome (hg38p13) using HISAT2 (https://ccb.jhu.edu/software/hisat2) . The FPKM value of each gene was calculated using Cufflinks (13), and the read counts of each gene were obtained by HTSeq-count (14). Differential expression analysis was performed using the DESeq (2012) R package (15). A P-value <0.05 and fold change >2 or fold

change <0.5 were set as the threshold for significantly differential expression. The heatmap and volcano plot were created using OmicStudio (https://www.omicstudio.cn).

ChIP-sequencing. DNA and protein cross-linking was achieved by adding 1% formaldehyde solution (cat. no. F8775; Sigma-Aldrich, Merck KGaA), followed by quenching the reaction with 125 mM glycine (included in a CHIP kit; cat. no. Bes5001; Bersinbio). Chromatin was extracted from the cross-linked cells using lysis buffer (included in a CHIP kit; cat. no. Bes5001; Bersinbio). The chromatin DNA was sonicated to obtain fragments ranging from 100 to 500 base pairs using MinElute PCR Purification Kit (cat. no. 28004; QIAGEN China Co., Ltd.). Immunoprecipitation of the chromatin DNA and antibody-associated beads was performed by incubating them overnight at 4˚C. The immunoprecipitated protein-DNA complexes were eluted from the Dynabeads (included in a CHIP kit; cat. no. Bes5001; Bersinbio) using an optimal method (https://v2.fangcloud.com/share/bcc477b7f13badd6dc7c0163a4). Sequencing libraries of the immunoprecipitated chromatin DNA were generated using the NEBNext® Ultra™ DNA Library Prep Kit for Illumina (New England BioLabs, Inc.). DNA purity and quantification were evaluated using a NanoDrop 2000 spectrophotometer (Thermo Fisher Scientific, Inc.). DNA integrity was assessed using the Agilent 2100 Bioanalyzer (Agilent Technologies, Inc.). The libraries underwent end repair, adaptor ligation, and removal of base U of the adaptor. After purification and size selection, the libraries were quantified using Qubit and the insert size was assessed using a high-sensitivity DNA chip. The libraries (12 pM) were sequenced on an Illumina NovaSeq 6000 platform using NovaSeq 6000 SP reagent kit (100 cycles; cat. no. 2002746; Illumina Inc.), generating 150 bp paired-end reads. The raw sequencing data in fastq format were processed using fastp software [FASTP (version 0.20.1) (https://github.com/OpenGene/fastp] to obtain clean reads by removing adapters, poly-N sequences, and low-quality reads. The clean reads were then mapped to the genome using Bowtie2 (16) and peaks were called using MACS2 (version 2.2.7.1) (17). The called peaks were visualized using IGV software and annotated using the ChIPseekerv (18) package in R. *De novo* and known motifs were identified using MEME-ChIP (version 4.9.1) (19), and GO enrichment analysis was performed using clusterProfiler (20).

Bioinformatic analyses. The pathways associated with HOXC10 in HNSCC were analyzed by Gene set enrichment analysis (GSEA) analysis with the R package ClusterProfiler (20). A total of 520 patients with HNSCC from TCGA database (https://portal.gdc.cancer.gov/) were divided into high and low expression groups based on HOXC10 expression, and the the median expression level of HOXC10 was set as the cut-off. Normalized enrichment score (NES), P-value, and false discovery rate (FDR) for all variables and signatures were obtained by running GSEA.

For m^{6}A site prediction, site-specific RNA adenosine methyltransferase peaks (SRAMP; http://www.cuilab.cn/sramp/) and RMBase_v2.0 (http://rna.sysu.edu.cn/rmbase/) were used.

Statistical analysis. GraphPad Prism 9 software (GraphPad Software, Inc.; Dotmatics) and Stata 13.0 (StataCorp LP) were used for the statistical analysis. All data represent the mean ± standard deviation (SD) of triplicate repeats. Student's unpaired t-test was used to compare two groups. The correlation between the two proteins was assessed using Pearson's correlation coefficient. Comparisons of three groups were performed using one-way analysis of variance (ANOVA) with Tukey's multiple comparison test. $P<0.05$ was considered to indicate a statistically significant difference.

Results

HOXC10 is overexpressed in HNSCC tissues and is associated with a poor prognosis. The sum of three pairs of cancer and adjacent tissues were first selected for RNA-seq and it was found that the expression of HOXC10 in HNSCC was increased (Fig. 1A and B), which was consistent with the results obtained from RT-qPCR and western blot analysis (Fig. 1C-E). HOXC10 expression was also upregulated in other cancer types, such as esophageal cancer (ESCA) and cervical squamous cell carcinoma and endocervical adenocarcinoma (CESC; Fig. 1F). Immunohistochemical staining of tissues from 77 patients with HNSCC revealed that HOXC10 expression was significantly higher in cancer tissues than in adjacent tissues (Fig. 1G). A high level of HOXC10 expression was markedly associated with advanced TNM stage (Table II), shorter survival times, and a higher rate of recurrence (Fig. 1H). These results demonstrated that HOXC10 is highly expressed in HNSCC tissues and is associated with a poor prognosis in patients with HNSCC.

In Table II, clinical stage IV included 40 patients with HNSCC, of which 28 had laryngeal cancer and 12 had hypopharyngeal cancer. It is crucial to note that among the 40 stage IV patients included in the present study, 38 were categorized as stage IVa, 2 were classified as stage IVb, and there were no cases of stage IVc. The patients with metastases are primarily characterized by neck lymph node involvement, and notably, there were no instances of distant metastases in the present study. Surgical management in cases of neck lymph node metastasis involved radical neck lymph node dissection, which has demonstrated the capability to achieve substantial removal of metastatic regions in the neck. Furthermore, the primary tumors of the stage IV patients were relatively large. The post-operative pathology reports indicated that 2 patients had positive margins. Thus, in the present study, surgery was found to effectively remove a significant portion of the tumors in most stage IV patients with HNSCC, but it may not completely remove tumors in all patients with stage IV disease.

High levels of HOXC10 promote HNSCC progression in vivo and in vitro. HOXC10 expression was revealed in five HNSCC cell lines and a normal nasopharyngeal epithelial cell line. As shown in Fig. 2A, HOXC10 expression in cancer cells was higher than in normal cells. Furthermore, HOXC10 was transfected with shRNAs into FaDu cells and HOXC10 vectors into Tu686 cells; transfection efficiencies were detected by RT-qPCR and western blotting (Fig. 2B and C). The migration and invasion assays revealed that HOXC10 knockdown inhibited the motility of FaDu cells. The EdU assay showed

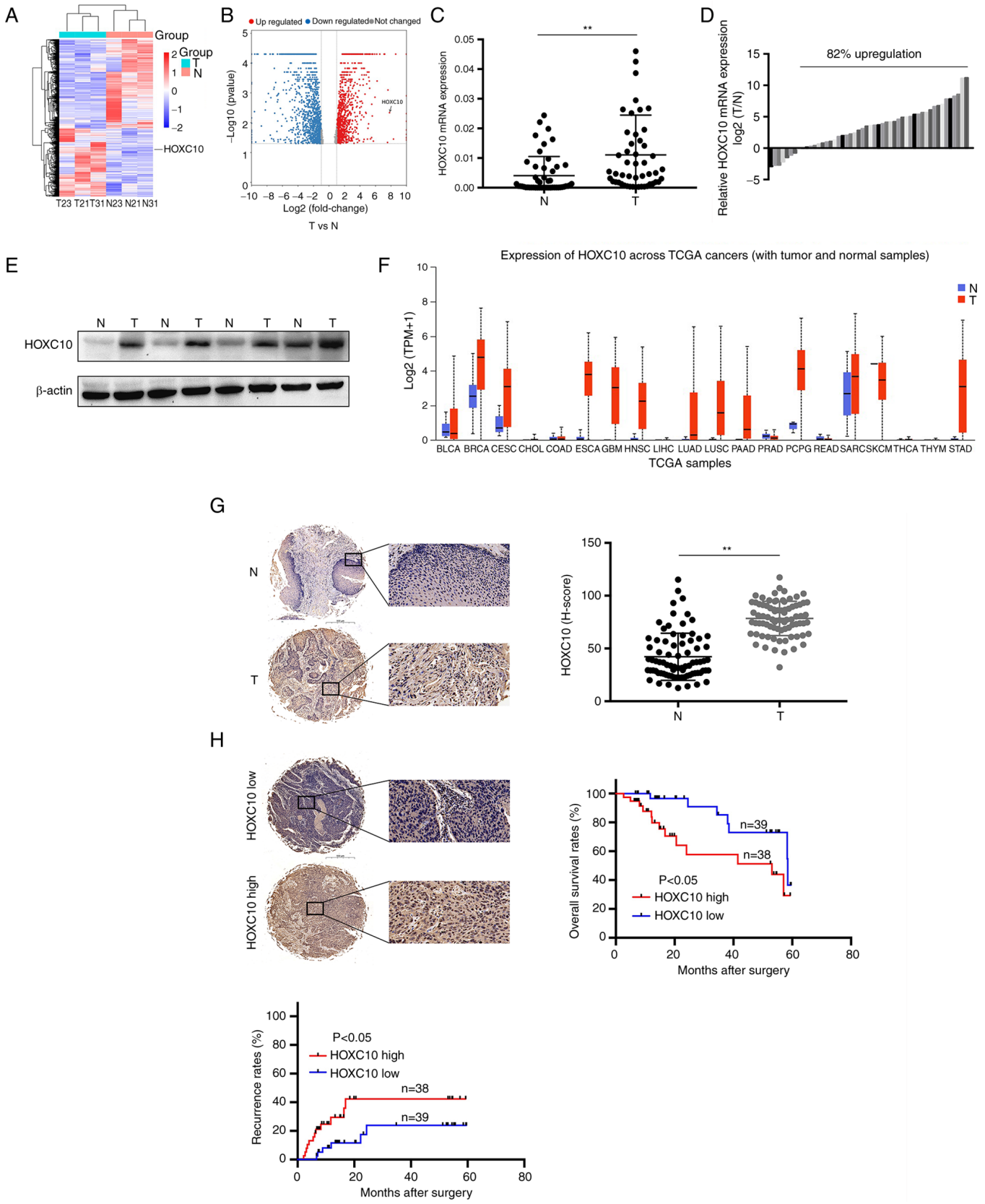

Figure 1. Overexpression of HOXC10 is positively correlated with the poor prognosis of patients with HNSCC. (A) RNA-seq was performed with three pairs of HNSCC and adjacent tissues. (B) Volcano plot of differentially expressed genes. Red represents upregulated genes, grey indicates genes not altered, and downregulated genes are in blue. (C and D) HOXC10 mRNA levels in 50 matched pairs of HNSCC and adjacent tissues were quantified using RT-qPCR. (E) Representative bands of HOXC10 protein levels in HNSCC and adjacent tissues. (F) The mRNA levels of HOXC10 in different types of cancer were analyzed using TCGA. (G) Immunohistochemistry was applied to assess the expression of HOXC10 in tissue microarrays, including 77 patients with HNSCC and representative images are presented. HOXC10 expression levels were analyzed by H-score. (H) Prognostic analysis of HOXC10 expression in 77 patients with HNSCC. **P<0.01. HOXC10, homeobox C10; HNSCC, head and neck squamous cell carcinoma; TCGA, The Cancer Genome Atlas Program; T, tumor; N, normal.

Table II. Association between HOXC10 and clinicopathological characteristics in 77 patients with head and neck squamous cell carcinoma.

Variables	No. of patients		P-value
	38 HOXC10^{high}	*39 HOXC10^{low}*	
Age (years)			
<65	17	21	
≥65	21	18	0.424
Smoking			
Yes	33	32	
No	5	7	0.562
Drinking			
Yes	19	24	
No	19	15	0.308
Hypertension			
Yes	13	12	0.747
No	25	27	
Tumor size (cm)			
<4	20	29	0.048
≥4	18	10	
Lymphatic metastasis			
Metastasis	19	15	
Nonmetastasis	19	24	0.308
Differentiation			
Moderate to poor	29	29	
High	9	10	0.842
Clinical stages			
I - III	14	23	0.016
IV	24	16	

P<0.05 was considered statistically significant. HOXC10, homeobox C10.

that knockdown of HOXC10 suppressed the cell growth rate of FaDu cells; by contrast, HOXC10 upregulation significantly promoted the migration, invasion, and growth rates of Tu686 cells (Fig. 2D-F). To analyze the function of HOXC10 *in vivo*, a subcutaneous xenograft model was established and a pulmonary metastasis model, as shown in Fig. 2G-J. FaDu-NC cells exhibited a higher proliferation ability than FaDu-shRNA2 cells; beyond that, the incidence of lung metastasis for FaDu-NC cells was higher than that of FaDu-shRNA2 cells (Fig. 2K). These results revealed that HOXC10 upregulation promotes HNSCC progression, both *in vivo* and *in vitro*.

EMT is widely recognized as an important event associated with cancer progression (21). The cellular morphology of the transfected HNSCC cells was detected and it was observed that FaDu-shRNA2 and Tu686-NC cells exhibited a cobblestone-like appearance such as epithelial cells, while FaDu-NC and Tu686-HOXC10 cells exhibited a spindle-like morphology such as fibroblasts (Fig. 3A). Next, it was found that knockdown of HOXC10 enhanced E-cadherin expression but reduced the expression of vimentin, N-cadherin and Snail in FaDu cells. Conversely, HOXC10 overexpression brought about the opposite changes in the expression of these EMT markers in Tu686 cells (Fig. 3B), which was further supported by immunofluorescence and immunohistochemical analyses (Fig. 3C-E). Taken together, these results indicated that HOXC10 could facilitate the progression of HNSCC by inducing EMT.

ADAM17 is a direct target of HOXC10 in HNSCC cells. To further investigate the target genes regulated by HOXC10, chromatin immunoprecipitation sequencing (ChIP-seq) was performed in Tu686-HOXC10 cells. To identify and annotate these target genes, MACS2 was introduced for peak calling filtered with the P-value and peak enrichment, and ChIPseeker was applied to annotate the peak regions in gene promoter regions following the promoter regions ranging from TSS 3,000 bp upstream to 3,000 bp downstream (Fig. 4A). As shown in Fig. 4B, peak regions in the whole genome were distributed as follows: 9.26% enrichment in the promoter regions, majority located introns (50.07%) and intergenic regions (33.7%), minority located in other regions including 0.71% downstream, 3.59% exons, 2.08% 3'UTR, and 0.58% 5'UTR. GO enrichment revealed that HOXC10 played

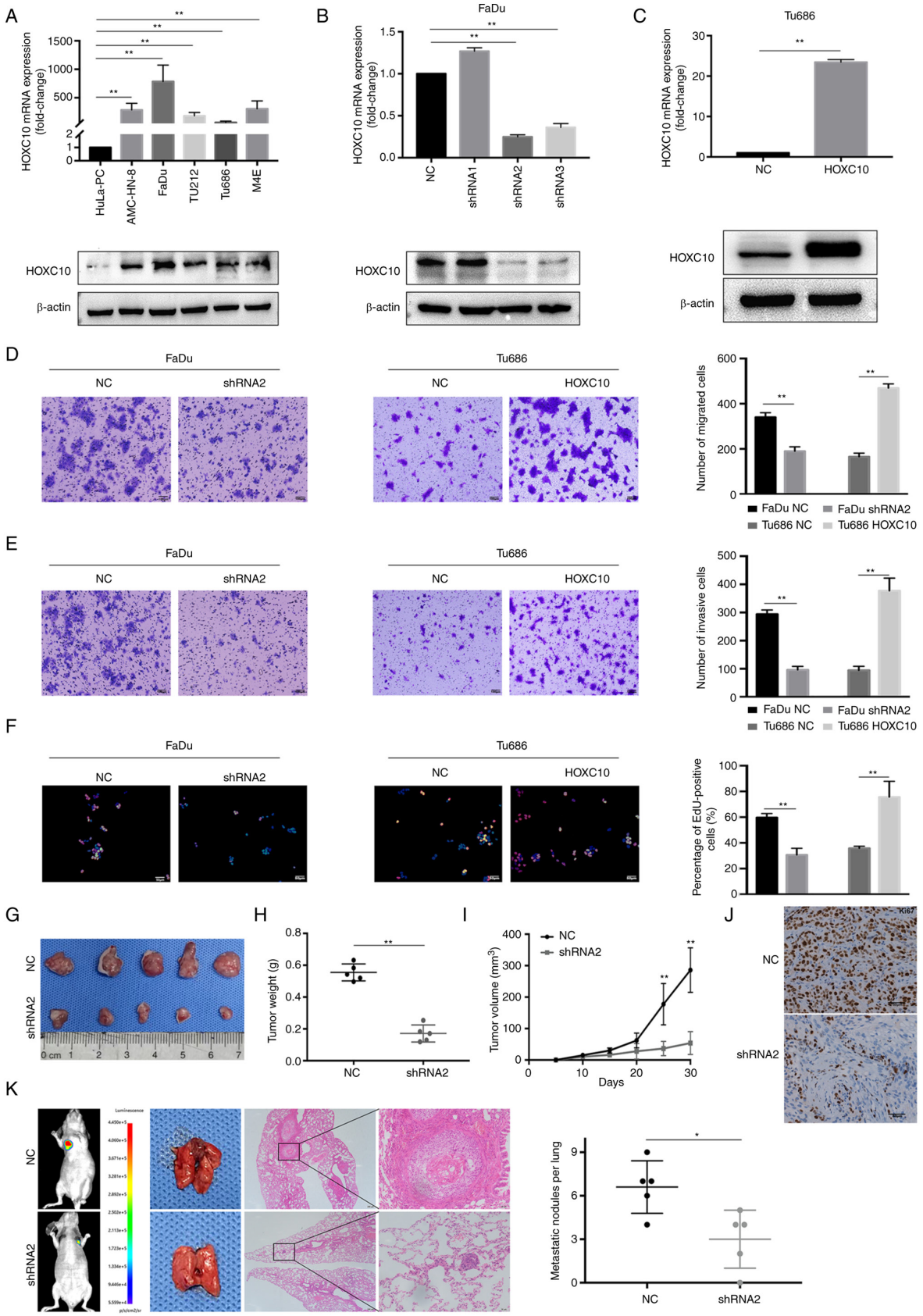

Figure 2. HOXC10 is involved in HNSCC cell migration, invasion, and proliferation in vitro and *in vivo*. (A) mRNA and protein levels of five HNSCC cell lines and a normal nasopharyngeal epithelial cell line. (B and C) The efficiency of transfection in the FaDu and Tu686 cell lines was verified by reverse transcription-quantitative PCR and western blot analysis. (D-F) Migration, invasion, and proliferation ability in transfected HNSCC cells were assessed by Transwell migration and EdU assays. Scale bar, 100 μm for D and E; scale bar, 50 μm for F. (G) Tumors derived from nude mice were subcutaneously transplanted with FaDu-NC and FaDu-shRNA2 cells. (H) Weight measurement of tumors. (I) Growth curves of subcutaneous tumors. (J) Ki67 expression was measured by immunohistochemistry. Scale bar, 50 μm. (K) Nude mice tails were intravenously injected with FaDu-NC and FaDu-shRNA2 cells to establish the pulmonary metastasis models; representative images show pulmonary metastases. Scale bar, 200 μm. **P<0.01. HOXC10, homeobox C10; HNSCC, head and neck squamous cell carcinoma; EdU, 5-ethynyl-2'-deoxyuridine; NC, negative controls; sh, small hairpin.

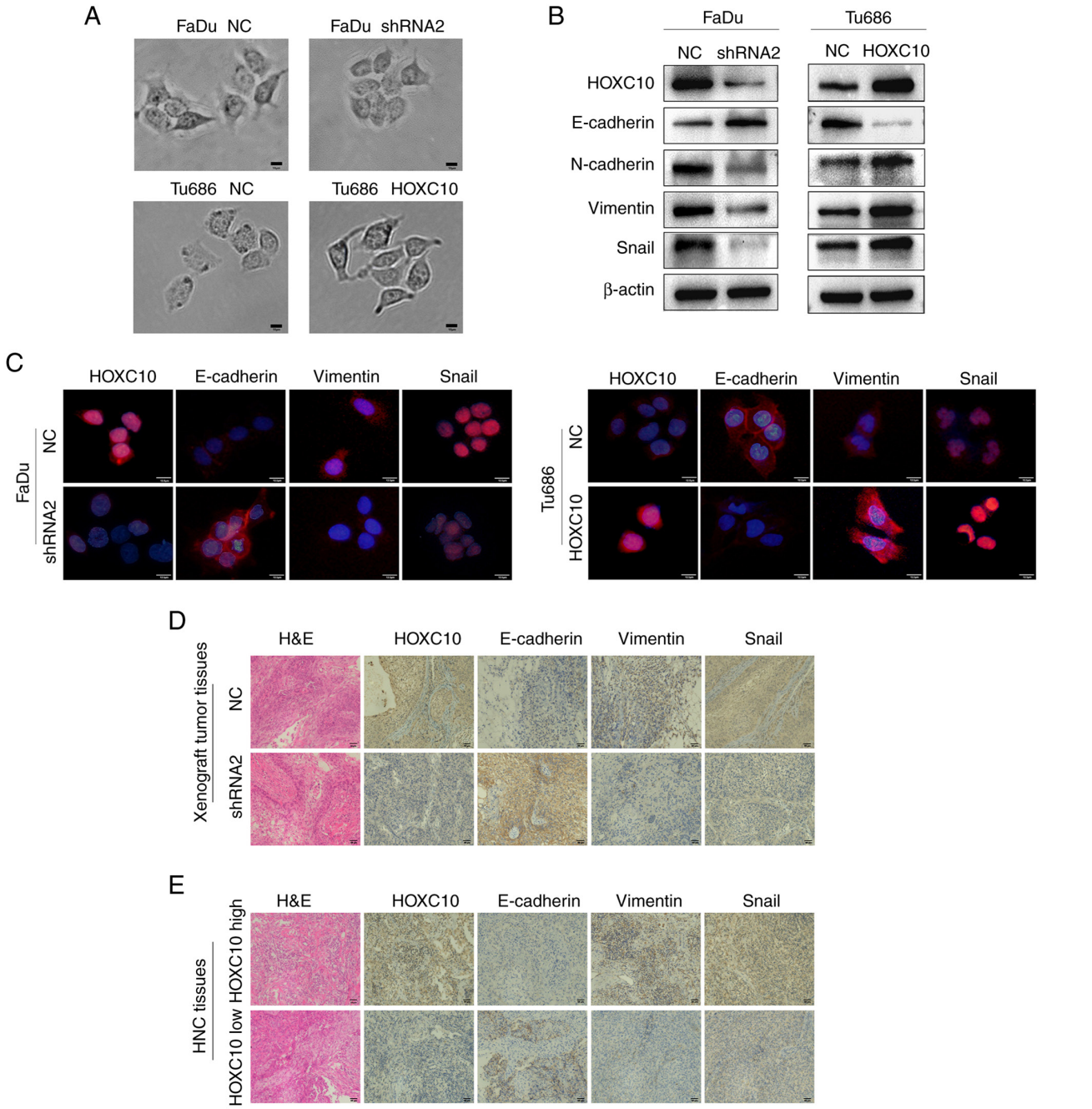

Figure 3. HOXC10 promotes cellular EMT in HNSCC. (A) The cellular morphology of the transfected HNSCC cells was detected. Scale bar, 10 μm. (B and C) Expression levels of EMT markers were analyzed by western blot analysis and immunofluorescence staining. Scale bar, 12.5 μm for C. (D and E) Immunohistochemical staining of EMT markers in serial sections of xenograft tumor and human HNSCC tissues. Scale bar, 50 μm. HOXC10, homeobox C10; EMT, epithelial-mesenchymal transition; HNSCC, head and neck squamous cell carcinoma; H&E, hematoxylin and eosin.

an important role in the 'epidermal growth factor receptor signaling pathway' (Fig. 4C). The metalloprotease, ADAM17 has been reported to activate ligands of EGFR and contribute to tumor progression (22). In the present study, it was found that a putative HOXC10-binding peak at the promoter region of the ADAM17 gene (Fig. 4D). Based on this, the potential motif bound by HOXC10 was also identified with MEME motif software (Fig. 4E). A dual-luciferase reporter assay revealed that HOXC10 enhanced the transcriptional activity of ADAM17 (Fig. 4F). Knockdown of HOXC10 reduced the expression of ADAM17 in FaDu cells; conversely, HOXC10 overexpression yielded the opposite effect in Tu686 cells (Fig. 4G and H). A previous study reported that ADAM17-EGFR signaling axis-dependent ERK activation mediated the proliferation of collecting duct kidney epithelial cells (23). In the present study, it was revealed that ADAM17 treatment significantly promoted the phosphorylation of EGFR and ERK1/2 in Tu686 cells (Fig. 4I). HOXC10 knockdown in FaDu cells suppressed the EGFR and ERK1/2 phosphorylation levels, which were restored after ADAM17 overexpression; by contrast, HOXC10 overexpression in Tu686 cells enhanced the phosphorylation of EGFR and ERK1/2, which was inhibited after ADAM17 knockdown (Fig. 4J). Correspondingly, HOXC10 knockdown restrained the growth rate of FaDu cells, which was regained after ADAM17

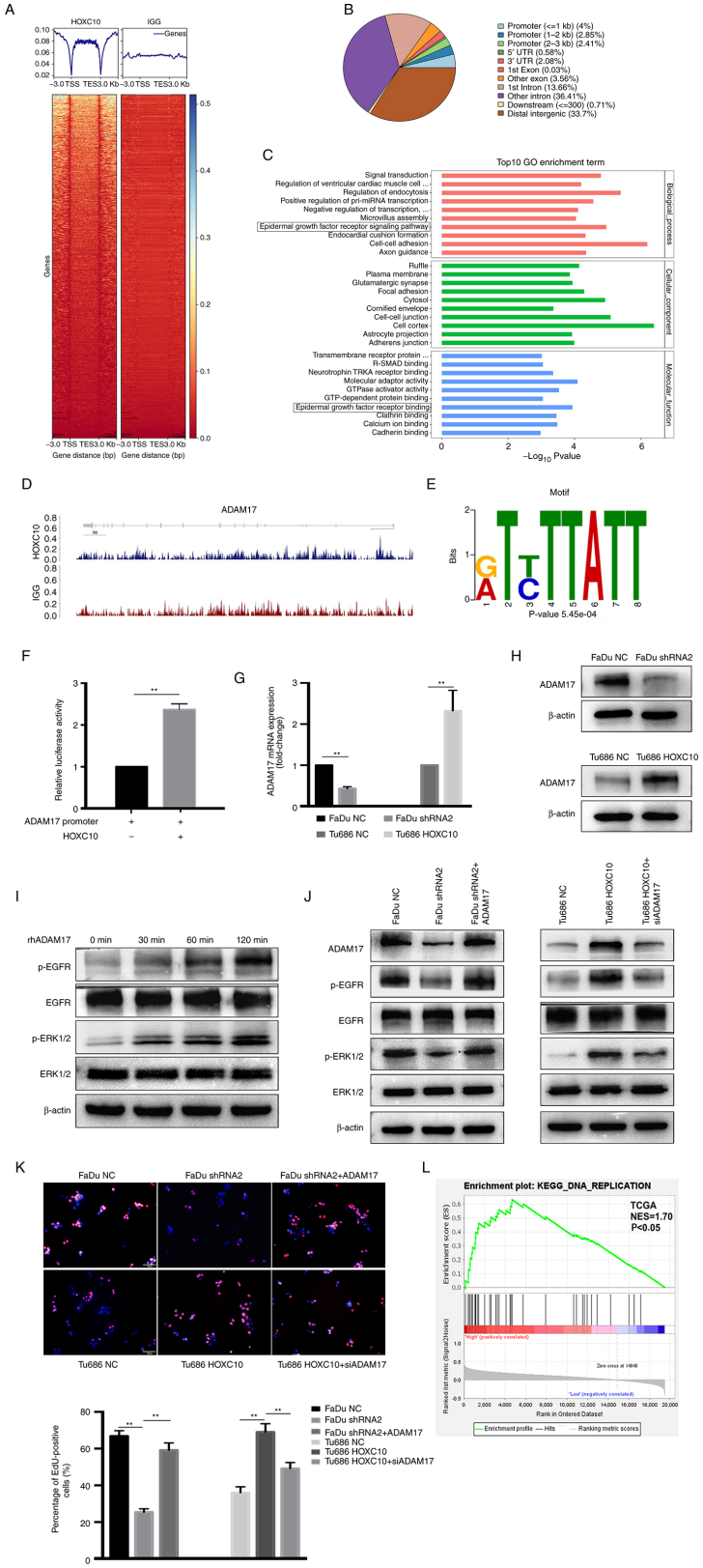

Figure 4. HOXC10 enhances the proliferation of HNSCC cells by targeting ADAM17. (A) Heat map of chromatin immunoprecipitation sequencing read densities around the HOXC10-bound regions 3 kb upstream of the TSS and 3 kb downstream of the TES. (B) Pie chart showing the distribution of HOXC10 peaks across the genome. (C) GO enrichment analysis of the top 10 biological processes, cellular components, and molecular function categories. (D) Distribution of HOXC10 binding peaks at ADAM17 promoters. (E) The ADAM17 promoter region contains a motif bound by HOXC10. (F) Transcriptional activity of ADAM17 was assessed by dual luciferase reporter assay. (G and H) Reverse transcription quantitative-PCR and western blot analyses were used to detect the expression of ADAM17 in the indicated cells. (I) Western blotting showed phosphorylation levels of EGFR and ERK1/2 in Tu686 cells treated with rhADAM17. (J) Phosphorylation levels of EGFR and ERK1/2 in the indicated cells were analyzed by western blotting. (K) The proliferation ability in transfected HNSCC cells was assessed by EdU assay. Scale bar, 50 μm. (L) GSEA, based on the TCGA dataset, showed that HOXC10 expression was positively associated with DNA replication. **P<0.01. HOXC10, homeobox C10; HNSCC, head and neck squamous cell carcinoma; ADAM17, a disintegrin and metalloproteinase 17; TSS, transcription start site; TES, transcription end site; GO, Gene Ontology; EGFR, epidermal growth factor receptor; EdU, 5-ethynyl-2'-deoxyuridine; GSEA, Gene Set Enrichment Analysis; TCGA, The Cancer Genome Atlas Program; KEGG, Kyoto Encyclopedia of Genes and Genomes.

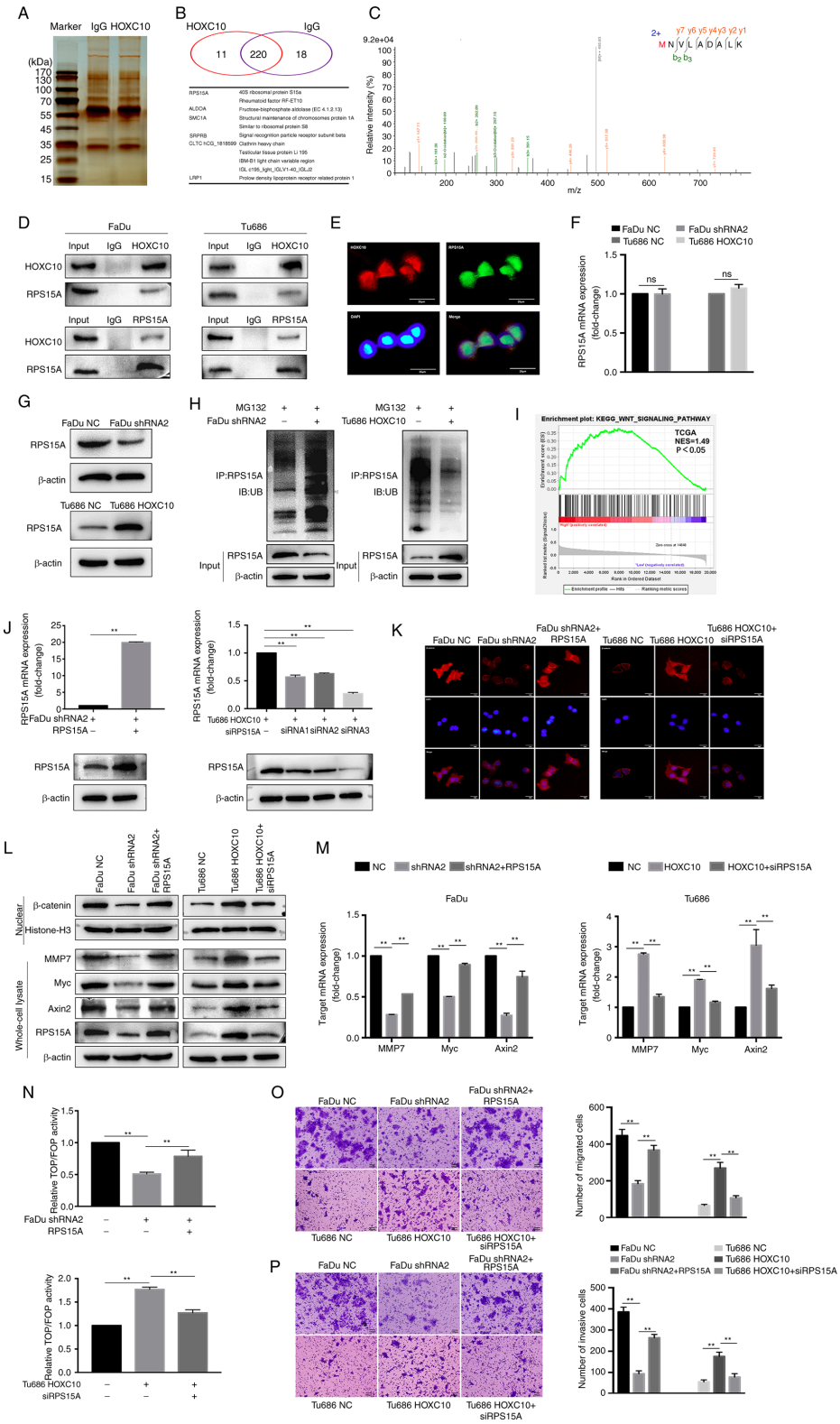

Figure 5. HOXC10 facilitates Wnt/β-catenin signaling in HNSCC by interacting with RPS15A. (A-C) The binding partners of HOXC10 were analyzed by the combination of Co-IP and mass spectrometric analyses, and 11 proteins are presented. (D) Co-IP and western blot analysis were used to verify the interaction between HOXC10 and RPS15A. (E) Immunofluorescence was used to identify the colocalization of HOXC10 and RPS15A. Scale bar, 25 μm. (F and G) RT-qPCR and western blot analysis of RPS15A expression in HNSCC cells transfected with shRNA2 or HOXC10. (H) Ubiquitination assay for the effects of HOXC10 on RPS15A ubiquitination. (I) GSEA based on the TCGA dataset suggested that HOXC10 expression was positively associated with the activation of the Wnt/β-catenin pathway. (J) The efficiency of transfection in the indicated cells was confirmed by RT-qPCR and western blotting. (K) Immunofluorescence detection of β-catenin in the nucleus after transfection with shRNA2, HOXC10, RPS15A, or siRPS15A in indicated cells. Scale bar, 25 μm. (L) Western blot analysis was performed to detect β-catenin, Myc, MMP7, Axin2, and RPS15A protein in HNSCC cells transfected with shRNA2, HOXC10, RPS15A, or siRPS15A. (M) Myc, MMP7, and Axin2 mRNA levels were analyzed by RT-qPCR in transfected HNSCC cells. (N) The activity of the Wnt/β-catenin pathway was analyzed by TOP/FOP-Flash luciferase reporter assay. (O and P) Migration and invasion ability in transfected HNSCC cells were assessed by Transwell assay. Scale bar, 100 μm **P<0.01. HOXC10, homeobox C10; HNSCC, head and neck squamous cell carcinoma; RPS15A, ribosomal protein S15A; Co-IP, co-immunoprecipation; RT-qPCR, reverse transcription quantitative-PCR; shRNA, short haipin RNA; siRPS15A, small interfering RPS15A; GSEA, Gene Set Enrichment Analysis; TCGA, The Cancer Genome Atlas Program.

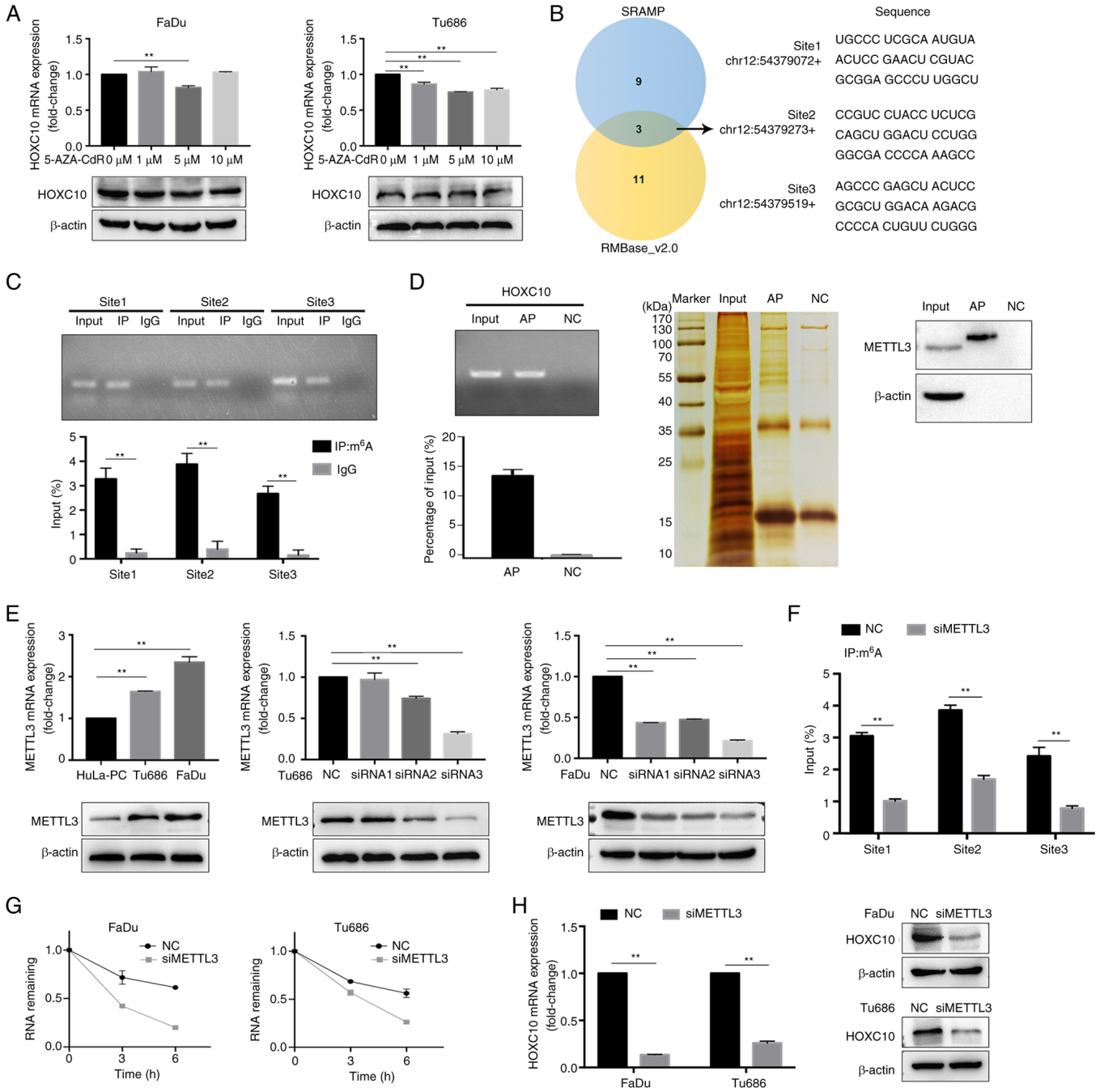

Figure 6. HOXC10 is modulated by m^{6}A RNA methylation. (A) HNSCC cells were treated with 5-AZA-CdR at different concentrations for 48 h, and the HOXC10 mRNA level was examined using RT-qPCR. (B) Predicted m^{6}A sites in HOXC10 mRNA from overlapping results of SRAMP and RMBase_ v2.0. (C) m^{6}A RIP-qPCR analysis showed that m^{6}A was highly enriched within the predicted m^{6}A sites in FaDu cells. (D) RAP-western blot assays indicated that HOXC10 mRNA interacted with METTL3. (E) HOXC10 mRNA and protein levels were analyzed by RT-qPCR and western blotting in the indicated HNSCC cells. (F) MeRIP assay for m^{6}A-modified HOXC10 mRNA in FaDu cells transfected with si-NC or si-METTL3. (G) HNSCC cells with METTL3 knockdown were treated with actinomycin D (5 μg/ml) for the indicated time points, and the HOXC10 mRNA level was examined by RT-qPCR. (H) HOXC10 mRNA and protein levels in HNSCC cells with METTL3 knockdown were detected by RT-qPCR and western blotting. **P<0.01. HOXC10, homeobox C10; m^{6}A, *N*^{6}-methyladenosine; HNSCC, head and neck squamous cell carcinoma; RT-qPCR, reverse transcription quantitative-PCR; RIP-qPCR, RNA immune precipitation-quantitative PCR; RAP, RNA antisense purification; METTL3, methyltransferase-like 3; MeRIP, methylated RNA immune precipitation; si-, small interfering; NC, negative control.

overexpression; HOXC10 overexpression enhanced the growth rate of Tu686 cells, which was suppressed after ADAM17 knockdown (Fig. 4K). Gene Set Enrichment Analysis (GSEA), based on the TCGA dataset, also indicated that HOXC10 expression was positively associated with 'DNA replication' (Fig. 4L). Collectively, these data demonstrated that HOXC10 promotes the proliferation of HNSCC via targeting the ADAM17/EGFR pathway.

HOXC10 facilitates Wnt/β-catenin signaling in HNSCC by interacting with RPS15A. To further explore the potential mechanism through which HOXC10 promotes the invasion

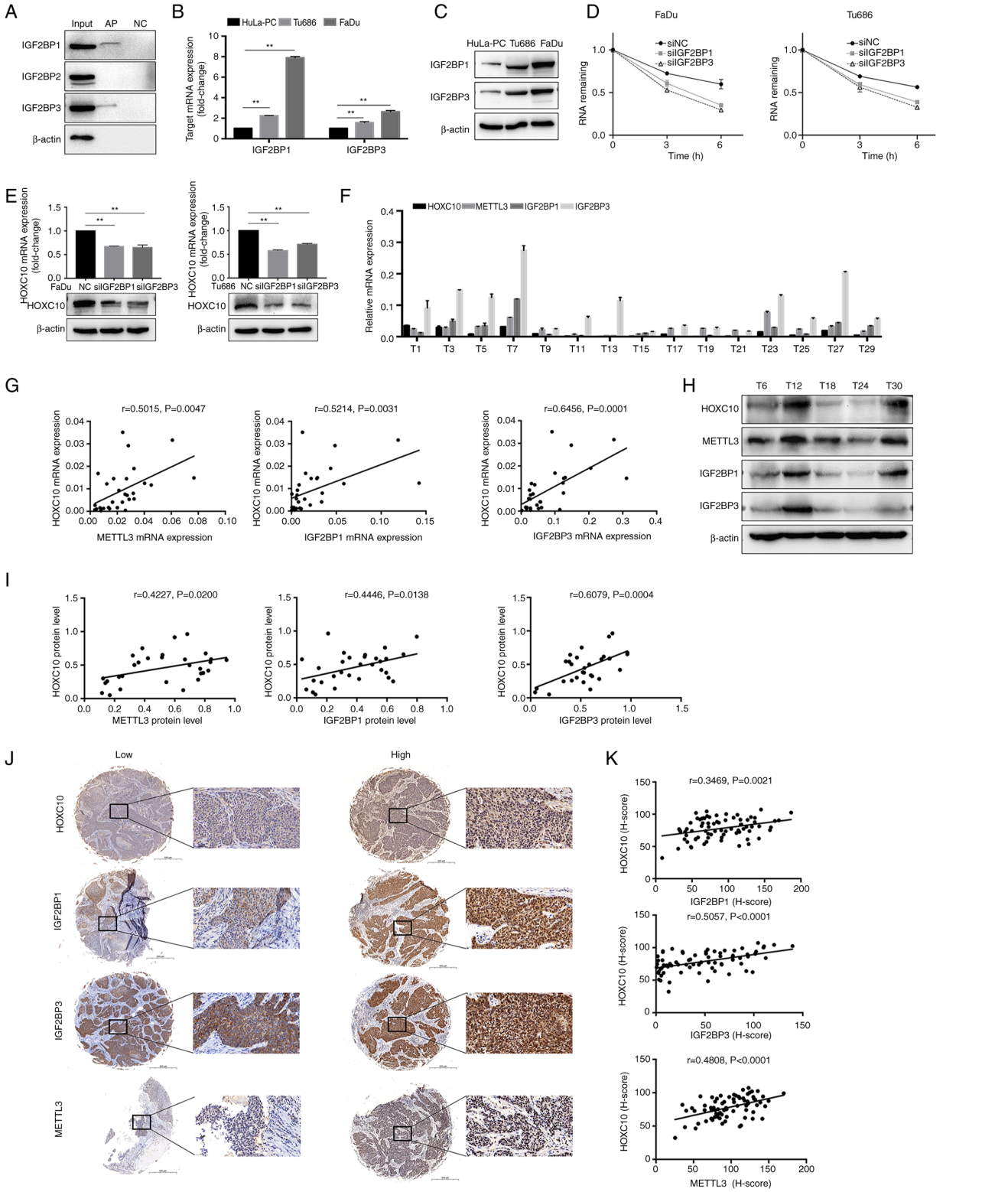

Figure 7. IGF2BP1 and IGF2BP3 participated in the recognition and stabilization of m^{6}A-modified HOXC10 mRNA. (A) The RAP-western blot assays indicated that HOXC10 mRNA interacted with IGF2BP1 and IGF2BP3. (B and C) IGF2BP1 and IGF2BP3 mRNA and protein levels were analyzed by RT-qPCR and western blotting in the indicated HNSCC cells. (D) HNSCC cells with IGF2BP1 or IGF2BP3 knockdown were treated with actinomycin D (5 μg/ml) for the indicated time points, and the HOXC10 mRNA level was examined by RT-qPCR. (E) HOXC10 mRNA and protein levels in HNSCC cells with IGF2BP1 or IGF2BP3 knockdown were detected by RT-qPCR and western blotting. (F) The mRNA expression of HOXC10, IGF2BP1, IGF2BP3, and METTL3 in 30 HNSCC tumor tissues was detected by RT-qPCR. A representative image is shown. (G) Pearson's correlation analysis between HOXC10 and IGF2BP1, IGF2BP3, or METTL3 was performed at the mRNA level. (H) The protein expression of HOXC10, IGF2BP1, IGF2BP3, and METTL3 in 30 HNSCC tumor tissues was detected by western blot analysis, and representative images are shown. (I) Pearson's correlation analysis between HOXC10 and IGF2BP1, IGF2BP3, or METTL3 was performed at the protein level. (J) Representative immunostaining images of HOXC10, IGF2BP1, IGF2BP3, and METTL3 in HNSCC tumor tissues. Scale bar, 500 μm. The enlarged image scale bar, 50 μm. (K) Correlation analysis of H-scores of HOXC10, IGF2BP1, IGF2BP3, and METTL3 using the Pearson's correlation coefficient. **P<0.01. IGF2BP1, insulin like growth factor 2 mRNA binding protein 1; IGF2BP3, insulin like growth factor 2 mRNA binding protein 3; m^{6}A, N^6-methyladenosine; HOXC10, homeobox C10; RAP, RNA antisense purification; RT-qPCR, reverse transcription quantitative-PCR; HNSCC, head and neck squamous cell carcinoma; METTL3, methyltransferase-like 3; NC, negative control.

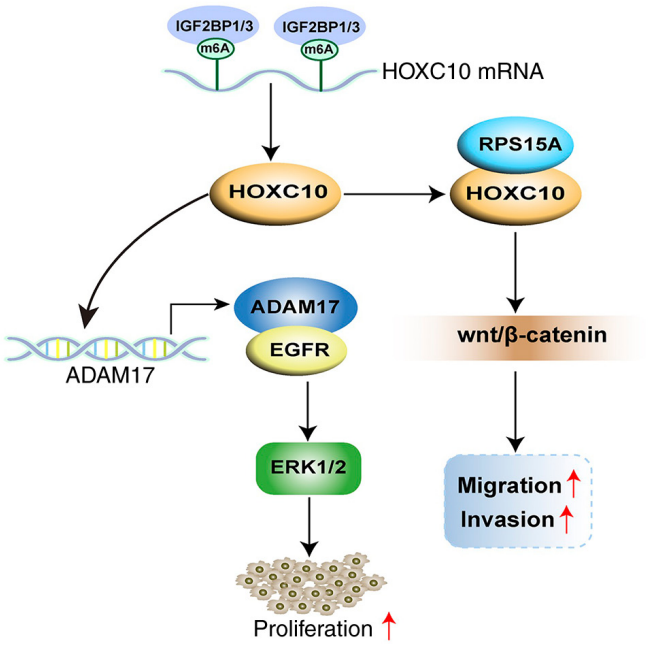

Figure 8. Proposed mechanism scheme of HOXC10 in HNSCC. A working model depicting that m^{6}A modification-mediated HOXC10 upregulation promotes proliferation and invasion of HNSCC cells by co-activation of ADAM17/EGFR and Wnt/β-catenin signaling. HOXC10, homeobox C10; HNSCC, head and neck squamous cell carcinoma; m^{6}A, N^6-methyladenosine; ADAM17, a disintegrin and metalloproteinase 17; EGFR, epidermal growth factor receptor; IGF2BP1/3, insulin like growth factor 2 mRNA binding protein 1/3; RPS15A, ribosomal protein S15A.

and metastasis of HNSCC, Co-IP and mass spectrometric (MS) analyses were performed to identify the underlying HOXC10-binding proteins in HNSCC cells. As shown in Fig. 5A-C, 11 proteins were identified among the candidate HOXC10-interacting partners. RPS15A was selected for further investigation, as prior studies have indicated that it is involved in the progression of gastric cancer and colorectal cancer (24-25), but its role in HNSCC has not been well studied. The interaction between HOXC10 and RPS15A was verified by co-IP and colocalization assays (Fig. 5D and E). Moreover, changes in the expression of HOXC10 did not influence RPS15A mRNA levels, whereas HOXC10 knockdown significantly downregulated RPS15A protein levels in FaDu cells, and overexpression of HOXC10 upregulated RPS15A protein levels in Tu686 cells (Fig. 5F and G). This indicated that HOXC10 influenced RPS15A expression at the protein level but not at the mRNA level. Ubiquitin-mediated proteolysis regulates protein stability without influencing mRNA levels and plays an important role in tumor progression (26). In the present study, it was hypothesized that the interaction between HOXC10 and RPS15A may regulate RPS15A proteolysis and thereby influence the protein level of RPS15A. As shown in Fig. 5H, ubiquitination assays showed that knockdown of HOXC10 obviously increased RPS15A ubiquitination after MG132 treatment; overexpression of HOXC10 produced the opposite effect. A previous study reported that RPS15A promoted angiogenesis in HCC by enhancing Wnt/β-catenin signaling (27). In the present study, GSEA based on the TCGA dataset demonstrated that HOXC10 expression was positively associated with genes upregulated by activation of the Wnt/β-catenin pathway (Fig. 5I). HOXC10 knockdown suppressed the expression levels of nuclear β-catenin and its downstream target genes, such as MMP7, Myc, and Axin2, which were partially restored by RPS15A overexpression; by contrast, HOXC10 overexpression or RPS15A knockdown yielded the opposite effect (Fig. 5J-M), which was then further confirmed by a TOP/FOP-Flash luciferase reporter assay (Fig. 5N). Additionally, it was observed that RPS15A overexpression restored cell migration and invasion impaired by HOXC10 knockdown in FaDu cells. RPS15A knockdown abrogated cell migration and invasion induced by HOXC10 overexpression in Tu686 cells (Fig. 5O and P). Taken together, these results indicated that HOXC10 interacts with RPS15A to facilitate the Wnt/β-catenin pathway activation and contribute to the invasion of HNSCC.

m^{6}A modification is associated with HOXC10 upregulation in HNSCC cells. Advances in tumor epigenetic regulation have shed light on the role of m^{6}A RNA methylation modification in tumor development and progression (28); whether HOXC10 is modulated by m^{6}A RNA methylation in HNSCC cells remains unclear. We found that the DNA methyltransferase inhibitor (5-Aza-CdR) failed to upregulate HOXC10 expression (Fig. 6A). m^{6}A modification has been reported to preferentially locate in the consensus motif 'RRm^{6}ACH' (R=G or A; H=A, C or U) (29), according to the results from online bioinformatics databases SRAMP and RMBase v2.0. The sum of three potential m^{6}A sequence motifs were found in HOXC10 mRNA (Fig. 6B). MeRIP analysis showed that m^{6}A was highly enriched within these predicted m^{6}A sites (Fig. 6C). As a crucial m^{6}A methyltransferase, METTL3 has been reported to play a significant role in catalyzing m^{6}A formation (30); RAP-western blot assays indicated that HOXC10 mRNA interacts with METTL3 (Fig. 6D). In addition, it was revealed that METTL3 expression was higher in HNSCC cells compared with HuLa-PC cells, and METTL3 knockdown reduced m^{6}A levels of HOXC10 mRNA (Fig. 6E and F). Notably, RNA stability assays demonstrated that METTL3 knockdown significantly decreased the stability of HOXC10 mRNA under actinomycin D treatment; knockdown of METTL3 resulted in a decrease in HOXC10 expression (Fig. 6G and H). These findings indicated that METTL3-mediated m^{6}A modification is associated with the upregulation of HOXC10 in HNSCC, probably by increasing the stability of its transcript.

Previous research reported that IGF2BPs could recognize m^{6}A modications in mRNA transcripts and enhance the stability and translation of these mRNAs (31); therefore, it was investigated whether IGF2BPs participate in the recognition and stabilization of m^{6}A-modified HOXC10 mRNA, and thereby regulate HOXC10 expression. As shown in Fig. 7A, the RAP-western blot assays showed that IGF2BP1 and IGF2BP3 bound to HOXC10 mRNA. IGF2BP1 or IGF2BP3 expression was higher in HNSCC cells compared to HuLA-PC cells (Fig. 7B-C). IGF2BP1 or IGF2BP3 knockdown decreased the stability of HOXC10 mRNA at different degrees after actinomycin D treatment (Figs. S2 and 7D). Moreover, knockdown of IGF2BP1 or IGF2BP3 resulted in a significant decrease in HOXC10 expression at both the mRNA and protein levels (Fig. 7E). These results indicated that IGF2BP1 and IGF2BP3 recognize and stabilize m^{6}A-tagged HOXC10

mRNA. Finally, the results of Pearson's correlation analysis, RT-qPCR and western blotting indicated that the expression level of HOXC10 was positively correlated with the levels of IGF2BP1, IGF2BP3, and METTL3 in HNSCC tissues, which was further supported by immunohistochemistry analysis in the tissue microarray (Fig. 7F-K).

Discussion

The present study demonstrated that HOXC10 is significantly elevated in HNSCC tissues, that a high level of HOXC10 is associated with the malignant phenotype of HNSCC, and that it is also an important prognostic factor for patients with HNSCC. The experimental approach combining CHIP-seq with MS analysis revealed the underlying mechanism by which HOXC10 promoted ADAM17 expression by binding its promoter region, and ADAM17/EGFR pathway activation facilitated the proliferation of HNSCC. Furthermore, HOXC10 interacted with RPS15A and enhanced RPS15A protein expression, which activated Wnt/β-catenin pathways and contributed to invasion and metastasis of HNSCC. Additionally, m^6A writer METTL3 regulated the m^6A modification of the HOXC10 transcript, and m^6A readers IGF2BP1 and IGF2BP3 participated in the recognizing and stabilizing of m^6A-tagged HOXC10 mRNA.

HOXC10 is a member of the HOX genes, which are a family of homeodomain transcription factors including HOXA, HOXB, HOXC, and HOXD (2). Previous studies have revealed that aberrant HOX gene expression plays a crucial role in the progression of human cancer. For example, the HOXA4/HOXB3 gene expression signature may be a biomarker of recurrence of high-grade serous ovarian cancer after cytoreductive surgery and adjuvant chemotherapy (32). The growth and metastasis of breast cancer may be regulated by the HMGA2/TET1/HOXA9 signaling pathway (33). HOXD9 promoted the invasion and metastasis of gastric cancer cells by transcriptional activation of RUFY3 (34). IL-1β induced HOXC10 upregulation and then promoted HCC metastasis by transactivating PDPK1 and VASP expression (35). In the present study, it was demonstrated that HOXC10 is overexpressed in HNSCC, and that HOXC10 overexpression endowed HNSCC cells with enhancement of proliferation, migration, and invasion abilities.

ADAM17, known as tumor necrosis factor-α (TNFα)-converting enzyme (TACE), is responsible for protease-driven shedding of membrane-tethered cytokines, cell surface receptors, and growth factors; among these, EGFR family ligands are included (36). The large number of substrates processed by ADAM17 renders it a key coordinator of numerous physiological and pathological processes, especially those related to the occurrence and development of cancer. For example, ADAM17 is overexpressed in diverse cancers, including colon carcinoma, breast cancer, hepatocellular carcinoma, and gastric cancer (37-40). ADAM17-mediated EGFR ligand shedding facilitated cancer cell invasion promoted by macrophages (22). Genetic, antibody-mediated, or pharmacological methods targeting ADAM17 prevented formation of metastases in the lung, suppressed tumor growth in various cancers, and have become a new strategy for advanced-stage cancer therapy (41-43). In the present study, to further investigate target genes regulated by HOXC10, ChIP-seq was performed. The results revealed that a putative HOXC10 binding site located at the promoter region of ADAM17, HOXC10, could enhance the transcriptional activity of ADAM17. Activation of ADAM17 by carcinogenic forms of Src has been reported to help promote tumorigenesis by enhancing signaling via EGFR and ERK in an autocrine and paracrine manner (44). Silencing ADAM17 may repress the activity of the EGFR/ERK pathway to reduce the proliferation of keloid fibroblasts (45). Consistently, the experiments that were conducted in the present study revealed that HOXC10 enhanced ADAM17 expression, increased the ADAM17-activated EGFR-ERK pathway, and contributed to the proliferation of HNSCC.

In order to explore the potential mechanism of HOXC10 in the progression of HNSCC more thoroughly, MS analysis was also applied, apart from ChIP-seq. Co-IP and MS confirmed a direct interaction between HOXC10 and RPS15A proteins. Notably, HOXC10 influenced RPS15A expression at the protein level but not the mRNA level. Previous studies have indicated that ubiquitin-mediated proteolysis regulates protein stability without influencing mRNA levels and plays an important role in tumor progression (46). In the present study, overexpression of HOXC10 decreased RPS15A ubiquitination and increased the protein level of RPS15A. HOXC10 itself does not belong to deubiquitinating enzymes; the HOXC10/RPS15A complex may influence the interaction between RPS15A and E3 ligase and thereby affect ubiquitin-mediated proteolysis of RPS15A. In future research, the mechanism through which HOXC10 regulates the ubiquitylation level of RPS15A, will be further analyzed. A previous study reported that RPS15A enhanced angiogenesis in HCC by enhancing Wnt/β-catenin signaling (27). RPS15A knockdown downregulated β-catenin expression and blocked the activation of Wnt signaling (47). In the present study, HOXC10 was demonstrated to influence RPS15A expression, HOXC10 knockdown supressed Wnt/β-catenin pathway activation, and RPS15A overexpression restored cell migration and invasion impaired by HOXC10 knockdown.

It is widely known that chemical modifications to human RNAs are involved in numerous pathophysiological processes, including cancer. Notably, N^6-methyladenosine (m^6A) modification, one of the most abundant post-translational mRNA internal modifications, participated in all stages of the RNA life cycle, such as RNA production and stability (48). m^6A modification is a dynamic and reversible biological process regulated by 'writers' (METTL3, METTL14, and WTAP), 'erasers' (FTO and ALKBH5), and 'readers' (YTH domain proteins and IGF2BPs) (49). The deposition of m^6A is encoded by writers (methyltransferases), which catalyze the formation of m^6A. Erasers (demethylases) selectively remove the m^6A code. Readers (specific RNA-binding proteins) decode m^6A methylation and modulate the m^6A progression (49). 'Writers', 'erasers', and 'readers' are frequently dysregulated in human cancers, which influence the expression of oncogene transcripts and oncoproteins (49). However, the relationship between m^6A modification and the oncogenic role of HOXC10 in HNSCC remains unclear. Recently, Wu *et al* (50) demonstrated that METTL3 alleviated human mesenchymal stem cell senescence through m^6A modification-dependent stabilization of the MIS12 transcript. Herein, the results of the present stydy showed that m^6A methylation was enriched within HOXC10 in HNSCC cells; moreover, METTL3 regulated the m^6A modification, and IGF2BP1 and IGF2BP3 participated in recognizing

and stabilizing the m^{6}A-modified HOXC10 transcript, thus affecting its mRNA expression. These results indicated that the upregulation of HOXC10 in HNSCC may be attributed to m^{6}A modification.

In the present study, the importance of HPV infection status is acknowledged as a clinically relevant parameter. However, a limitation due to the absence of routine preoperative HPV testing must be noted in the clinical protocol of the present study, which prevented the authors from including HPV data in Table II. Future studies with HPV infection status assessment could provide valuable insights into its potential implications, and its incorporation in the analyses of the present study will be considered when such data becomes available.

In conclusion, HOXC10 was demonstrated to be overexpressed in HNSCC, and m^{6}A modification-mediated HOXC10 upregulation promoted proliferation and invasion of HNSCC cells by co-activation of ADAM17/EGFR and Wnt/β-catenin signaling (Fig. 8). Therefore, HOXC10 may be a novel marker and a potential therapeutic strategy for HNSCC.

Acknowledgements

Not applicable.

Funding

The present study was supported by grants from the National Natural Science Foundation of China (grant no. 81972529), the Science and Technology Commission of Shanghai Municipality (grant no. 19411961300), and the Shanghai Sailing Program (grant no. 23YF1404700).

Availability of data and materials

The datasets used and/or analysed during the present study are available from the corresponding author on reasonable request. The original RNA-seq data has been deposited in the NCBI Sequence Read Archive (SRA) with the associated accession number PRJNA1033223 (https://www.ncbi.nlm.nih.gov/bioproject/PRJNA1033223). The original CHIP-seq data has been deposited in the NCBI SRA with the associated accession number PRJNA1033205 (https://www.ncbi.nlm.nih.gov/bioproject/PRJNA1033205).

Authors' contributions

LZ and CX conceived and designed the project. YZ, QH and CW conducted the experiments. YZ, QH, CW collected the clinical samples and data. YZ, QH and CW performed the statistical analysis. LZ, CX and YX provided technical and material support. YX and YG performed language editing. LZ, YZ, YG and XY reviewed and revised the manuscript. YZ, YG, XY and YX assembled the figures. YG and XY confirm the authenticity of all the raw data. All authors approved the final version of the manuscript.

Ethics approval and consent to participate

All animal procedures and patient experiments were approved (approval no. 202212201) by the Eye and ENT Hospital, Fudan University (Shanghai, China). The present study was approved (approval no. 2018036) by the Ethics Committee of the Fudan University Eye and ENT Hospital. All patients provided written informed consent.

Patient consent for publication

Not applicable.

Competing interests

The authors declare that they have no competing interests.

References

1. Sung H, Ferlay J, Siegel RL, Laversanne M, Soerjomataram I, Jemal A and Bray F: Global cancer statistics 2020: GLOBOCAN estimates of incidence and mortality worldwide for 36 cancers in 185 countries. CA Cancer J Clin 71: 209-249, 2021.
2. Taketani T, Taki T, Shibuya N, Kikuchi A, Hanada R and Hayashi Y: Novel NUP98-HOXC11 fusion gene resulted from a chromosomal break within exon 1 of HOXC11 in acute myeloid leukemia with t(11;12)(p15;q13). Cancer Res 62: 4571-4574, 2002.
3. Malek R, Gajula RP, Williams RD, Nghiem B, Simons BW, Nugent K, Wang H, Taparra K, Lemtiri-Chlieh G, Yoon AR, *et al*: TWIST1-WDR5-*Hottip* regulates *Hoxa9* chromatin to facilitate prostate cancer metastasis. Cancer Res 77: 3181-3193, 2017.
4. Stavnes HT, Holth A, Don T, Kærn J, Vaksman O, Reich R, Trope' CG and Davidson B: HOXB8 expression in ovarian serous carcinoma effusions is associated with shorter survival. Gynecol Oncol 129: 358-363, 2013.
5. Miyazaki YJ, Hamada J, Tada M, Furuuchi K, Takahashi Y, Kondo S, Katoh H and Moriuchi T: HOXD3 enhances motility and invasiveness through the TGF-beta-dependent and -independent pathways in A549 cells. Oncogene 21: 798-808, 2002.
6. de Stanchina E, Gabellini D, Norio P, Giacca M, Peverali FA, Riva S, Falaschi A and Biamonti G: Selection of homeotic proteins for binding to a human DNA replication origin. J Mol Biol 299: 667-680, 2000.
7. Pathiraja TN, Nayak SR, Xi Y, Jiang S, Garee JP, Edwards DP, Lee AV, Chen J, Shea MJ, Santen RJ, *et al*: Epigenetic reprogramming of HOXC10 in endocrine-resistant breast cancer. Sci Transl Med 6: 229ra241, 2014.
8. Tan Z, Chen K, Wu W, Zhou Y, Zhu J, Wu G, Cao L, Zhang X, Guan H, Yang Y, *et al*: Overexpression of HOXC10 promotes angiogenesis in human glioma via interaction with PRMT5 and upregulation of VEGFA expression. Theranostics 8: 5143-5158, 2018.
9. Livak KJ and Schmittgen TD: Analysis of relative gene expression data using real-time quantitative PCR and the 2(-Delta Delta C(T)) method. Methods 25: 402-408, 2001.
10. Wang SH, Zhu XL, Wang F, Chen SX, Chen ZT, Qiu Q, Liu WH, Wu MX, Deng BQ, Xie Y, *et al*: LncRNA H19 governs mitophagy and restores mitochondrial respiration in the heart through Pink1/Parkin signaling during obesity. Cell Death Dis 12: 557, 2021.
11. Zhang H, Zhu Q, Ji Y, Wang M, Zhang Q, Liu W, Li R, Zhang J, Xu P, Song X and Lv C: hucMSCs treatment prevents pulmonary fibrosis by reducing circANKRD42-YAP1-mediated mechanical stiffness. Aging (Albany NY) 15: 5514-5534, 2023.
12. National Research Council (US) Committee for the Update of the Guide for the Care and Use of Laboratory Animals: Guide for the care and use of laboratory animals. 8th edition. National Academies Press, Washington DC, 2011.
13. Trapnell C, Roberts A, Goff L, Pertea G, Kim D, Kelley DR, Pimentel H, Salzberg SL, Rinn JL and Pachter L: Differential gene and transcript expression analysis of RNA-seq experiments with TopHat and Cufflinks. Nat Protoc 7: 562-578, 2012.
14. Anders S, Pyl PT and Huber W: HTSeq-a python framework to work with high-throughput sequencing data. Bioinformatics 31: 166-169, 2015.
15. Love M, Anders S and Huber W: Differential analysis of RNA-Seq data at the gene level using the DESeq2 package. Heidelberg: European Molecular Biology Laboratory (EMBL), 2013. https://bioconductor.org/help/course-materials/2013/EMBOBGI/DESeq2_parathyroid.pdf.

16. Langmead B and Salzberg SL: Fast gapped-read alignment with Bowtie 2. Nat Methods 9: 357-359, 2012.
17. Zhang Y, Liu T, Meyer CA, Eeckhoute J, Johnson DS, Bernstein BE, Nusbaum C, Myers RM, Brown M, Li W and Liu XS: Model-based analysis of ChIP-Seq (MACS). Genome Biol 9: R137, 2008.
18. Yu G, Wang LG and He QY: ChIPseeker: An R/Bioconductor package for ChIP peak annotation, comparison, and visualization. Bioinformatics 31: 2382-2383, 2015.
19. Bailey TL, Boden M, Buske FA, Frith M, Grant CE, Clementi L, Ren J, Li WW and Noble WS: MEME SUITE: Tools for motif discovery and searching. Nucleic Acids Res 37: W202-W208, 2009.
20. Yu G, Wang LG, Han Y and He QY: clusterProfiler: An R package for comparing biological themes among gene clusters. OMICS 16: 284-287, 2012.
21. Huang Y, Hong W and Wei X: The molecular mechanisms and therapeutic strategies of EMT in tumor progression and metastasis. J Hematol Oncol 15: 129, 2022.
22. Gnosa SP, Puig Blasco L, Piotrowski KB, Freiberg ML, Savickas S, Madsen DH, Auf dem Keller U, Kronqvist P and Kveiborg M: ADAM17-mediated EGFR ligand shedding directs macrophage-promoted cancer cell invasion. JCI Insight 7:e155296, 2022.
23. Beck Gooz M, Maldonado EN, Dang Y, Amria MY, Higashiyama S, Abboud HE, Lemasters JJ and Bell PD: ADAM17 promotes proliferation of collecting duct kidney epithelial cells through ERK activation and increased glycolysis in polycystic kidney disease. Am J Physiol Renal Physiol 307: F551-F559, 2014.
24. Liu T, Zhang J, Chen H, Bianba T, Pan Y, Wang X, Jiang Y and Yang Z: PSMC2 promotes the progression of gastric cancer via induction of RPS15A/mTOR pathway. Oncogenesis 11: 12, 2022.
25. Zheng Z, Cui H, Wang Y and Yao W: Downregulation of RPS15A by miR-29a-3p attenuates cell proliferation in colorectal carcinoma. Biosci Biotechnol Biochem 83: 2057-2064, 2019.
26. Wei CY, Zhu MX, Yang YW, Zhang PF, Yang X, Peng R, Gao C, Lu JC, Wang L, Deng XY, *et al*: Downregulation of RNF128 activates Wnt/β-catenin signaling to induce cellular EMT and stemness via CD44 and CTTN ubiquitination in melanoma. J Hematol Oncol 12: 21, 2019.
27. Guo P, Wang Y, Dai C, Tao C, Wu F, Xie X, Yu H, Zhu Q, Li J, Ye L, *et al*: Ribosomal protein S15a promotes tumor angiogenesis via enhancing Wnt/β-catenin-induced FGF18 expression in hepatocellular carcinoma. Oncogene 37: 1220-1236, 2018.
28. Wu Y, Yang X, Chen Z, Tian L, Jiang G, Chen F, Li J, An P, Lu L, Luo N, *et al*: m^{6}A-induced lncRNA RP11 triggers the dissemination of colorectal cancer cells via upregulation of Zeb1. Mol Cancer 18: 87, 2019.
29. Csepany T, Lin A, Baldick CJ Jr and Beemon K: Sequence specificity of mRNA N6-adenosine methyltransferase. J Biol Chem 265: 20117-20122, 1990.
30. Zeng C, Huang W, Li Y and Weng H: Roles of METTL3 in cancer: Mechanisms and therapeutic targeting. J Hematol Oncol 13: 117, 2020.
31. Huang H, Weng H, Sun W, Qin X, Shi H, Wu H, Zhao BS, Mesquita A, Liu C, Yuan CL, *et al*: Recognition of RNA N^6-methyladenosine by IGF2BP proteins enhances mRNA stability and translation. Nat Cell Biol 20: 285-295, 2018.
32. Miller KR, Patel JN, Zhang Q, Norris EJ, Symanowski J, Michener C, Sehouli J, Braicu I, Destephanis DD, Sutker AP, *et al*: HOXA4/HOXB3 gene expression signature as a biomarker of recurrence in patients with high-grade serous ovarian cancer following primary cytoreductive surgery and first-line adjuvant chemotherapy. Gynecol Oncol 149: 155-162, 2018.
33. Sun M, Song CX, Huang H, Frankenberger CA, Sankarasharma D, Gomes S, Chen P, Chen J, Chada KK, He C and Rosner MR: HMGA2/TET1/HOXA9 signaling pathway regulates breast cancer growth and metastasis. Proc Natl Acad Sci USA 110: 9920-9925, 2013.
34. Zhu H, Dai W, Li J, Xiang L, Wu X, Tang W, Chen Y, Yang Q, Liu M, Xiao Y, *et al*: HOXD9 promotes the growth, invasion and metastasis of gastric cancer cells by transcriptional activation of RUFY3. J Exp Clin Cancer Res 38: 412, 2019.
35. Dang Y, Chen J, Feng W, Qiao C, Han W, Nie Y, Wu K, Fan D and Xia L: Interleukin 1β-mediated HOXC10 overexpression promotes hepatocellular carcinoma metastasis by upregulating PDPK1 and VASP. Theranostics 10: 3833-3848, 2020.
36. Grötzinger J, Lorenzen I and Düsterhöft S: Molecular insights into the multilayered regulation of ADAM17: The role of the extracellular region. Biochim Biophys Acta Mol Cell Res 1864: 2088-2095, 2017.
37. Blanchot-Jossic F, Jarry A, Masson D, Bach-Ngohou K, Paineau J, Denis MG, Laboisse CL and Mosnier JF: Up-regulated expression of ADAM17 in human colon carcinoma: Co-expression with EGFR in neoplastic and endothelial cells. J Pathol 207: 156-163, 2005.
38. Gao MQ, Kim BG, Kang S, Choi YP, Yoon JH and Cho NH: Human breast cancer-associated fibroblasts enhance cancer cell proliferation through increased TGF-α cleavage by ADAM17. Cancer Lett 336: 240-246, 2013.
39. Tsai WC, Hsu PW, Lai TC, Chau GY, Lin CW, Chen CM, Lin CD, Liao YL, Wang JL, Chau YP, *et al*: MicroRNA-122, a tumor suppressor microRNA that regulates intrahepatic metastasis of hepatocellular carcinoma. Hepatology 49: 1571-1582, 2009.
40. Shou ZX, Jin X and Zhao ZS: Upregulated expression of ADAM17 is a prognostic marker for patients with gastric cancer. Ann Surg 256: 1014-1022, 2012.
41. Bolik J, Krause F, Stevanovic M, Gandraß M, Thomsen I, Schacht SS, Rieser E, Müller M, Schumacher N, Fritsch J, *et al*: Inhibition of ADAM17 impairs endothelial cell necroptosis and blocks metastasis. J Exp Med 219: e20201039, 2022.
42. Ye J, Yuen SM, Murphy G, Xie R and Kwok HF: Anti-tumor effects of a 'human & mouse cross-reactive' anti-ADAM17 antibody in a pancreatic cancer model in vivo. Eur J Pharm Sci 110: 62-69, 2017.
43. Huang L, Chen J, Quan J and Xiang D: Rosmarinic acid inhibits proliferation and migration, promotes apoptosis and enhances cisplatin sensitivity of melanoma cells through inhibiting ADAM17/EGFR/AKT/GSK3β axis. Bioengineered 12: 3065-3076, 2021.
44. Maretzky T, Zhou W, Huang XY and Blobel CP: A transforming Src mutant increases the bioavailability of EGFR ligands via stimulation of the cell-surface metalloproteinase ADAM17. Oncogene 30: 611-618, 2011.
45. Le X and Fan YF: ADAM17 regulates the proliferation and extracellular matrix of keloid fibroblasts by mediating the EGFR/ERK signaling pathway. J Plast Surg Hand Surg 57: 129-136, 2023.
46. Peng R, Zhang PF, Yang X, Wei CY, Huang XY, Cai JB, Lu JC, Gao C, Sun HX, Gao Q, *et al*: Overexpression of RNF38 facilitates TGF-β signaling by ubiquitinating and degrading AHNAK in hepatocellular carcinoma. J Exp Clin Cancer Res 38: 113, 2019.
47. Liang J, Liu Y, Zhang L, Tan J, Li E and Li F: Overexpression of microRNA-519d-3p suppressed the growth of pancreatic cancer cells by inhibiting ribosomal protein S15A-mediated Wnt/β-catenin signaling. Chem Biol Interact 304: 1-9, 2019.
48. Zaccara S, Ries RJ and Jaffrey SR: Reading, writing and erasing mRNA methylation. Nat Rev Mol Cell Biol 20: 608-624, 2019.
49. Lan Q, Liu PY, Haase J, Bell JL, Hüttelmaier S and Liu T: The critical role of RNA m^{6}A methylation in cancer. Cancer Res 79: 1285-1292, 2019.
50. Wu Z, Shi Y, Lu M, Song M, Yu Z, Wang J, Wang S, Ren J, Yang YG, Liu GH, *et al*: METTL3 counteracts premature aging via m^{6}A-dependent stabilization of MIS12 mRNA. Nucleic Acids Res 48: 11083-11096, 2020.